Uniform semiclassical methods of analyzing undulations in far-wing line spectra

R. J. Bieniek
Department of Astronomy and Division of General Studies, University of Illinois at Urbana-Champaign, Urbana, Illinois 61801
(Received 18 October 1976)

Two uniform, semiclassical methods are presented for analytically evaluating matrix elements using stationary-phase techniques. The analytic expressions are appropriate for electronic transitions between molecular states that have monotonic difference potentials. Such a situation is encountered in the calculation of the spectra in excimer (e.g., Xe_2^*) and excimer-like (e.g., RbXe*) vapor systems. One method utilizes uniform JWKB wave functions throughout the analytic evaluation of the matrix elements, while the second uses simple JWKB wave functions that are modified at the end. The first proves to be more accurate for such systems. The uniform nature of its derivation assures its applicability even to transitions that occur near classical turning points. Numerical results are presented for the far red-wing emission spectrum of RbXe, and a detailed interpretive analysis of the undulatory structure is given. Using the uniform-JWKB, stationary-phase approximation, modifications of the RbXe*($A\,^2\Pi_{1/2}$) potential are suggested based on a comparison of the predicted and experimental spectra.

I. INTRODUCTION

In the past few years, undulations in the far wings of collisionally broadened spectral lines have been experimentally resolved in gaseous alkali-metal noble-gas systems.[1-3] The process involves electronic transitions between the intermolecular potentials that form during the collision. Correspondingly, considerable interest has been generated in theoretical methods of dealing with the underlying process. The aim has been to develop semiclassical techniques that remain valid when classical methods break down.[4]

When a classical analysis predicts an infinite intensity (such as at classical satellites), a stationary-phase analysis using simple JWKB wave functions will often yield reasonable results.[3-7] However, this technique is not valid when a stationary-phase point is near a classical turning point of the collision. In such situations, the amplitude of the simple JWKB wave function becomes infinite; this is a bothersome problem.

We can overcome this difficulty by using uniform JWKB wave functions, which are valid both close to, and far from, classical turning points.[8] However, when these are used, the analytic evaluation of matrix-element integrals by the method of stationary phase often becomes intractable. Child has presented such an evaluation for the case where there is an extremum in the intermolecular difference potential, although some steps in his derivation are not completely clear.[9] This corresponds to two points of stationary phase in the integral.

The purpose of this paper is to present a uniform method of evaluating T-matrix integrals with single points of stationary phase, using uniform JWKB wave functions. The result will be called the uniform-JWKB stationary-phase approximation. Far red-wing photoemission from an attractive to a repulsive potential is typical of a general class of processes for which this method is applicable. This is the lasing transition in excimer (excited-dimer) lasers, such as Xe_2^* and KrF*, which are under active consideration for applications in laser-induced fusion.[10-12] Numerical results from the uniform JWKB uniform approximation will be presented for the far red-wing of the 7948-Å atomic line of Rb collisionally broadened by Xe perturbers. This is completely analogous to true excimer systems, and was chosen because both theoretical and experimental information is available.[2]

II. BASIC THEORY

The total emission rate of photons per unit frequency interval per unit densities of the initial colliding nuclear species is[13]

$$\frac{d^2N}{dtd\nu}(E_i,\lambda) = (512\pi^4/3\hbar^2k_i)\lambda^{-3}\mu \sum_{L=0}^{L_{\max}} (2L+1)\left|T_{fi}^L\right|^2 , \quad (1)$$

where $L_{\max}=\infty$. The subscripts designate channels (i for initial, f for final). L is the total orbital angular momentum of the nuclei. ν is the frequency, λ is the wavelength, and μ is the reduced mass. k_i is the asymptotic wave number of the nuclei in the initial channel; i.e., $k_i^2=2\mu E_i/\hbar^2$. T_{fi}^L is the T-matrix element of the radial wave functions:

$$T_{fi}^L=\int_0^\infty \psi_f^L(R)M(R)\psi_i^L(R)dR . \quad (2)$$

R is the radial distance between the two nuclei. $M(R)$ is the transition moment; in the processes considered here, $M(R)=D(R)$, the dipole-coupling element. $\psi_c^L(R)$ is the partial-wave radial wave function of channel c with angular momentum L. It is asymptotically normalized to

$$\psi_c^L(R)=k_c^{-1/2}\sin(k_cR-\tfrac{1}{2}L\pi+\eta_c^L)\ . \tag{3}$$

In using Eq. (2) as the T-matrix element, we have implicitly averaged over changes of nuclear angular momentum, which is a good approximation in most situations. The differential emission intensity is related to the production rate by

$$I_\nu(E_i,\lambda)\equiv\frac{dI}{d\nu}(E_i,\lambda)=h\nu\,\frac{d^2N}{dtd\nu}(E_i,\lambda)\ . \tag{4}$$

III. UNIFORM JWKB UNIFORM APPROXIMATION

In the straightforward semiclassical analysis, the quantal radial wave functions in Eq. (2) for the T-matrix element are replaced by simple JWKB wave functions[8]

$$\psi_c^L(R)=A_c^L(R)\sin[\phi_c^L(R)+\tfrac{1}{4}\pi]\ , \tag{5a}$$

where

$$A_c^L(R)=[k_c^L(R)]^{-1/2}\ , \tag{5b}$$

$$k_c^L(R)=\left|K_c^L(R)^2\right|^{1/2}\ , \tag{5c}$$

$$\phi_c^L(R)=\int_{R_c^t}^{R}k_c^L(r)dr\ , \tag{5d}$$

$$K_c^L(R)^2=(2\mu/\hbar^2)[E-V_c(R)]+(L+\tfrac{1}{2})^2/R^2\ . \tag{5e}$$

R_c^t is the classical turning point of colliding nuclei in channel c; it satisfies $K_c^L(R_c^t)^2=0$. In what follows, the channel and angular momentum identifiers, c and L, will not be explicitly indicated, unless confusion would result.

Unfortunately, in the region around the classical turning point, the simple JWKB wave function "blows up" due to the amplitude (or modulus) factor, $A_c^L(R)$. To avoid this problem, one can use the uniform JWKB wave function[8]

$$\psi(R)=\pi^{1/2}[x(R)/K(R)^2]^{1/4}\mathrm{Ai}[x(R)]\ , \tag{6a}$$

where

$$x(R)=-q\left|\tfrac{3}{2}\phi(R)\right|^{2/3} \tag{6b}$$

and

$$q=\begin{cases}+1 & \text{if } R>R^t,\ [K^L(R)^2>0],\\ -1 & \text{if } R<R^t,\ [K^L(R)^2<0].\end{cases}$$

This wave function is uniformly valid both near to and far from the classical turning point. For $R\gg R^t$, the uniform JWKB wave function [Eq. (6)] approaches the form of the simple JWKB wave function [Eq. (5)]. For $R\approx R^t$, the uniform wave function attains the form of the "exact" seimclassical solution for a linear fit to the effective potential in the region around the turning point. For the potential $V(R^t)+V'(R^t)\Delta R$, where $\Delta R=R-R^t$, the appropriate wave function is[14]

$$\xi(R)=\pi^{1/2}U^{-1/6}\mathrm{Ai}(-U^{1/3}\Delta R)\ , \tag{7a}$$

where

$$U=-(2\mu/\hbar^2)V'(R^t)\ . \tag{7b}$$

The number of primes denote the order of differentiation. This is the solution that the uniform wave function approaches. This is not quite the exact wave function of the linear potential in the quantal sense because the Airy function is not zero at $R=0$. However, for realistic potentials it will be quite small and effectively zero. The use of the term "exact" in the discussion that follows will have this implicit qualification.

By comparing Eqs. (6) and (7), we can define an effective classical turning point $\overline{R}^t$ and slope $\overline{U}$ that convert the uniform JWKB wave function [Eq. (6a)] into the form of the exact solution of the linear potential [Eq. (7a)]. These satisfy the relations

$$\overline{R}^t(R)=R-q[x(R)^3K(R)^{-2}]^{1/2}\ , \tag{8a}$$

$$\overline{U}(R)=[K(R)^2/x(R)]^{3/2}\ . \tag{8b}$$

Equation (8) also implies the corollary relations

$$K^2(R)=\overline{U}(R)\Delta\overline{R}(R)\ , \tag{9a}$$

$$\phi(R)=\tfrac{2}{3}q\overline{U}(R)^{1/2}\left|\Delta\overline{R}(R)\right|^{3/2}\ , \tag{9b}$$

where

$$\Delta\overline{R}(R)=R-\overline{R}^t(R)\ . \tag{9c}$$

The uniform JWKB wave function [Eq. (6)] can now be written in the form of

$$\psi(R)=\pi^{1/2}\overline{U}(R)^{-1/6}\mathrm{Ai}[-\overline{U}(R)^{1/3}\Delta\overline{R}(R)]\ . \tag{10}$$

The dependence of these functions on the variable R will not be explicitly indicated in what follows, unless it is required for clarity.

With the wave function in this form, the T-matrix element can be analytically evaluated by the method of stationary phase. Unlike prior methods,[4-7] the result will be valid when the stationary-phase point is close to or far from the classical turning points. By substituting Eq. (10) into Eq. (2), we have

$$T_{fi}=\int_{-\infty}^{\infty}\pi M(R)(\overline{U}_f\overline{U}_i)^{-1/6}\mathrm{Ai}(-\overline{U}_f^{1/3}\Delta\overline{R}_f)\times\mathrm{Ai}(-\overline{U}_i^{1/3}\Delta\overline{R}_i)dR\ . \tag{11}$$

The lower integration limit has been extended from 0 to $-\infty$ because the Airy functions are effectively zero in that region for realistic situations. By writing the homogeneous Airy function in its integral form[15]

$$\mathrm{Ai}[-(3a)^{-1/3}x] = (2\pi)^{-1}(3a)^{1/3} \times \int_{-\infty}^{\infty} \exp[i(at^3 - xt)]\,dt \ ; \qquad (12)$$

Eq. (11) becomes

$$T_{fi} = \pi \iiint_{-\infty}^{\infty} M(R)(\bar{U}_f \bar{U}_i)^{-1/6}(2\pi)^{-2}(\bar{U}_f \bar{U}_i)^{-1/3} \times \exp[\, iF(x,y,R\,|\,R)]\,dx\,dy\,dR \ , \qquad (13a)$$

where

$$F(x,y,R\,|\,p) = \frac{x^3}{3\bar{U}_f(p)} - Rx + \bar{R}_f^t(p)x + \frac{y^3}{3\bar{U}_i(p)} - Ry + \bar{R}_i^t(p)y \ . \qquad (13b)$$

The stationary-phase point, R_s, is located where

$$\left.\frac{\partial F}{\partial x}\right|_{R=p=R_s} = \left.\frac{\partial F}{\partial y}\right|_{R=p=R_s} = \left.\frac{\partial F}{\partial R}\right|_{R=p=R_s} = 0 \ . \qquad (14)$$

Around this value of the internuclear separation, the exponential is slowly varying, and the major contribution to the T-matrix element occurs. On solving Eq. (14), we find

$$R_s = (\bar{U}_f \bar{R}_f^t - \bar{U}_i \bar{R}_i^t)/\Delta\bar{U}_{fi} \ , \qquad (15)$$

where $\Delta\bar{U}_{fi} = \bar{U}_f - \bar{U}_i$. By using Eq. (9), we see this implies that the local wave number (and thus kinetic energy) remains unchanged during the electronic transition at the stationary-phase point

$$k_f(R_s) = k_i(R_s) \ . \qquad (16)$$

This simply means that the transitions are vertical. Equation (16) is equivalent to the condition

$$\Delta V_{if}(R_s) = \epsilon \ , \qquad (17)$$

where $\Delta V_{if}(R) = V_i(R) - V_f(R)$ is the intermolecular difference potential, and $\epsilon = h\nu$ is the energy of the photon. We restrict ourselves to situations for which there is only a single unique solution to Eq. (17) for each ϵ; i.e., $\Delta V_{if}(R)$ is monotonic. Its inverse, $R(\Delta V_{fi})$ is single valued.

The exponential in Eq. (13a) is replaced by $F(x,y,R\,|\,R_s)$ and the other functions are set to their values at $R = R_s$. The T-matrix element then becomes

$$T_{fi} = \pi M(R_s)[\bar{U}_f(R_s)\bar{U}_i(R_s)]^{-1/6} \times \int_{-\infty}^{\infty} \mathrm{Ai}\{-\bar{U}_f(R_s)^{1/3}[R - \bar{R}_f^t(R_s)]\} \times \mathrm{Ai}\{-\bar{U}_i(R_s)^{1/3}[R - \bar{R}_i^t(R_s)]\}\,dR \ . \qquad (18)$$

Using Eq. (A5) of the Appendix, the integration of Eq. (18) can be accomplished to give

$$T_{fi} = \pi M(R_s)[\bar{U}_f(R_s)\bar{U}_i(R_s)]^{-1/2} \times \{[1/\bar{U}_i(R_s)] - [1/\bar{U}_f(R_s)]\}^{-1/3} \times \mathrm{Ai}(-\{[1/\bar{U}_i(R_s)] - [1/\bar{U}_f(R_s)]\}^{-1/3}\Delta\bar{R}_{fi}^t(R_s)), \qquad (19a)$$

where

$$\Delta\bar{R}_{fi}^t(R) = \bar{R}_f^t(R) - \bar{R}_i^t(R) \ . \qquad (19b)$$

From Eq. (15), one can show that $\Delta\bar{R}_i(R_s) = U_f\Delta\bar{R}_{fi}^t/\Delta\bar{U}_{fi}$ and $\Delta\bar{R}_f(R_s) = \Delta\bar{U}_i\Delta\bar{R}_f^t/\Delta\bar{U}_{fi}$. Using these relations, the argument of the Airy function simplifies to $-q\,|\tfrac{3}{2}\Delta\phi_{fi}(R_s)|^{2/3}$, with $\Delta\phi_{fi}(R) = \phi_f(R) - \phi_i(R)$. One can also simplify the coefficient of the Airy function by noting that $k_c'(R) = \tfrac{1}{2}q\bar{U}_c^{1/2} \times |\Delta\bar{R}_c|^{-1/2}$ and that

$$\Delta k_{fi}'(R_s) = qK(R_s)^2\Delta\phi_{fi}(R_s)[3\phi_f(R_s)\phi_i(R_s)]^{-1},$$

where $\Delta k_{fi}'(R) = k_f'(R) - k_i'(R)$. $k(R_s)$ is the common local wave number at the stationary-phase point, i.e., $k(R_s) = k_i(R_s) = k_f(R_s)$. With these results, we can write the T-matrix element of Eq. (19a) as

$$T_{fi} = \pi M(R_s)k(R_s)^{-1}\,|2\Delta k_{fi}'(R_s)|^{-1/2} \times |\tfrac{3}{2}\Delta\phi_{fi}(R_s)|^{1/6}\mathrm{Ai}[-q\,|\tfrac{3}{2}\Delta\phi_{fi}(R_s)|^{2/3}] \ . \qquad (20)$$

An analogous result was obtained by Miller in an investigation of curve-crossing effects.[16] Equation (20) is the uniform-JWKB stationary-phase approximation for single points of stationary phase. It is applicable whether the stationary-phase point is near to or far from the classical turning point. It is also valid whether the stationary point is in the classically allowed or classically forbidden region of the potentials (which is the purpose of the parameter q).

Equation (20) has the correct limiting behavior as the stationary-phase point approaches the classical turning points. In this case, the potential in the region between becomes progressively more linear in realistic situations. Since this equation is exact for linear potentials, it has the correct form in the limiting case. When the stationary-phase point is far from the turning points, $\Delta\phi_{fi}(R_s)$ is large [because $V_f(R)$ and $V_i(R)$ are not parallel]. Using the first-order asymptotic form of $\mathrm{Ai}(-x)$ for large x,[15] we have

$$T_{fi} \sim \pi^{1/2} M(R_s) k(R_s)^{-1} \left| 2\Delta k'_{fi}(R_s) \right|^{-1/2} \times \sin[\Delta\phi_{fi}(R_s) + \tfrac{1}{4}\pi] , \tag{21}$$

for $R_s \gg R_c$.

This can be compared to the asymptotic result one obtains using simple JWKB wave functions [Eq. (5)] in the stationary-phase method. These should be adequate in the asymptotic domain. Using a cubic fit to $\Delta\phi_{fi}(R)$ around the stationary-phase point, the analytic evaluation of T_{fi} gives[7]

$$T_{fi} = \tfrac{1}{2}\pi [f(R_s) - f'(R_s)\Delta\phi''_{fi}/\Delta\phi'''_{fi}] \times \left| \tfrac{1}{2}\Delta\phi'''_{fi} \right|^{-1/3} [\cos(u)\mathrm{Ai}(y) - p\sin(u)\mathrm{Gi}(y)] + \tfrac{1}{2}\pi f'(R_s) \left| \tfrac{1}{2}\Delta\phi''' \right|^{-2/3} \times [\sin(u)\mathrm{Ai}'(y) + p\cos(u)\mathrm{Gi}'(y)] , \tag{22a}$$

where

$$f(R) = M(R) A_i(R) A_f(R) , \tag{22b}$$

$$u = \Delta\phi_{fi} + (\Delta\phi''_{fi})^3/[3(\Delta\phi'''_{fi})^2] , \tag{22c}$$

$$y = -\left| \tfrac{1}{2}\Delta\phi'''_{fi} \right|^{-4/3} (\tfrac{1}{2}\Delta\phi''_{fi})^2 , \tag{22d}$$

$$p = \begin{cases} +1 & \text{if } \Delta\phi''_{fi}\Delta\phi'''_{fi} \geq 0 , \\ -1 & \text{if } \Delta\phi''_{fi}\Delta\phi'''_{fi} < 0 . \end{cases} \tag{22e}$$

$\Delta\phi_{fi}$ and its derivatives are to be evaluated at the stationary-phase point R_s. $\mathrm{Gi}(y)$ is the bounded, inhomogeneous Airy function.[15,17] For the situation set up in the uniform method, we find $p = 1$ in Eq. (22a). For simple JWKB wave function, $A_c(R)$ is given by Eq. (5b). In the asymptotic domain $f'(R) \ll f(R)$. Using the first-order expansion of $\mathrm{Gi}(y)$ for large negative y, we find the asymptotic form of the T-matrix element in the cubic approximation is

$$T_{fi} \sim \tfrac{1}{2}\pi M(R_s) k(R_s)^{-1} \left| \tfrac{1}{2}\Delta\phi'''_{fi} \right|^{-1/3} \pi^{-1/2} \left| \tfrac{1}{2}\Delta\phi'''_{fi} \right|^{1/3} \times \left| \tfrac{1}{2}\Delta\phi''_{fi} \right|^{-1/2} \sin(u + \tfrac{2}{3}y^{3/2} + \tfrac{1}{4}\pi) \tag{23a}$$

$$= \pi^{1/2} M(R_s) k(R_s)^{-1} \left| 2\Delta k'_{fi}(R_s) \right|^{-1/2} \times \sin[\Delta\phi_{fi}(R_s) + \tfrac{1}{4}\pi] . \tag{23b}$$

This is in agreement with the uniform result [Eq. (21)].

We would expect the cubic formula [Eq. (22)] to be inapplicable near classical turning points because only simple JWKB wave functions were used in its derivation. However, the cubic analysis can be used near such extrema if we employ modified JWKB wave functions. These have the form of Eq. (5a), but the amplitude is given by

$$\bar{A}_c(R) = \pi^{1/2} \left| x(R) K(R)^{-2} \right|^{1/4} [\mathrm{Ai}(-x)^2 + \mathrm{Bi}(-x)^2]^{1/2} , \tag{24a}$$

and the phase by

$$\bar{\phi}_c(r) = \tfrac{1}{4}\pi - \theta(x) , \tag{24b}$$

where $x(R)$ is given by Eqs. (6b) and (5d), and

$$\theta(x) = \arctan[\mathrm{Bi}(-x)/\mathrm{Ai}(-x)] . \tag{24c}$$

This makes the modified JWKB wave function numerically equal to the uniform JWKB wave function. Using the method of comparison equations with uniform solutions, we find $d/dR = k(R) x(R)^{-1/2} d/dx$.[8] Using this and the relations[15]

$$\frac{d\theta}{dx} = -\frac{1}{\pi}[\mathrm{Ai}(-x)^2 + \mathrm{Bi}(-x)^2]^{-1} , \tag{25a}$$

$$\frac{d^2\theta}{dx^2} = -2\pi[\mathrm{Ai}(-x)\mathrm{Ai}'(-x) + \mathrm{Bi}(-x)\mathrm{Bi}(-x)] \left(\frac{d\theta}{dx}\right)^2 , \tag{25b}$$

$$\frac{d^3\theta}{dx^3} = 2\frac{d\theta}{dx}\left[\frac{3}{4}\left(\frac{d^2\theta}{dx^2} \Big/ \frac{d\theta}{dx}\right)^2 - \left(\frac{d\theta}{dx}\right)^2 + x\right], \tag{25c}$$

we can determine the derivatives of the modified amplitudes and phases needed in the cubic formula. These modifications are of practical importance only if $\phi_c(R) \lesssim 7.8$; for larger values $\bar{\phi}_c(R) = \phi_c(R) \pm 0.001$ (in rad). With these modifications, the cubic analysis remains finite near classical turning points.

A numerical comparison was made between the modified cubic formula and the uniform formula for a linear potential; the uniform approach is semiclassically exact for this situation. The stationary-phase points were again chosen to be where $k_i(R_s) = k_f(R_s)$. This is no longer the correct condition for the modified JWKB integral since the phases no longer have the simple form of Eq. (5d). However, since the determination of the true stationary phase point would be somewhat impractical, the approximate point was utilized. When the stationary-phase point was near the classical turning point, the modified cubic result differed by as much as a factor of three from the uniform result. There are three obvious sources of this discrepancy. Firstly, $\Delta\bar{\phi}'''(R_s)$ of the modified phases gets large near a turning point, indicating a cubic analysis is probably not sufficient. This is to be expected, since we are forcing the wave function into the unnatural form of a sine function rather than an Airy function. Secondly, by using the approximate stationary phase point determined from Eq. (17), rather then the true one determined from $\Delta\bar{\phi}'(R_s) = 0$, we must introduce some error. However, even with these deficiencies, the modified cubic analysis reproduced rather well the positions of the extrema and zeros of the T-matrix elements as a function of

stationary-phase point.

The third source of error is due to an inherent approximation used in the cubic analysis. In this and related approaches, an exponential term involving the sum of phases is neglected in the integrand of the T-matrix integral.[5,7] It is assumed its contribution averages to zero because of rapid oscillations. In the uniform analysis, no terms are ignored. This is not a minor point because its effects show up even in the asymptotic region. For large, but typical, values of $R_s - R_c^t$, the cubic results differed by as much as 25% from the uniform values. This is significant since the simple JWKB wave functions used in the derivation are accurate in this domain. But as was the case near the classical turning point, the cubic analysis reproduces the positions of the extrema and zeroes.

From these considerations, we conclude that the uniform evaluation of T-matrix elements by the method of stationary phase is significantly superior to those employing simple or modified JWKB wave functions. However, the modified JWKB cubic approximation does have its usefulness. The uniform result presented here should be more accurate than the cubic in regions where realistic potentials are fairly linear. It is not obvious that it should be superior in other cases, such as near a parabolic centrifugral barrier. A uniform-JWKB stationary-phase approximation is not available for this situation. In contrast though, the modified cubic analysis can utilize the moduli and phases of Weber parabolic cylinder functions, which are more accurate.[8,18] Since the present research indicates that the modified cubic analysis gives informative numerical and structural results even near turning points, it can be tailored to give useful information in a variety of situations. However, for the particular process considered in Sec. IV, the uniform approximation is expected to give more accurate results due to the form of the potentials.

IV. FAR RED-WING LINE BROADENING IN Rb-Xe

The transition from the $5^2P_{1/2}$ to $5^2S_{1/2}$ atomic levels of Rb produces a spectral line at 7948 Å. During a collision with Xe, an excited Rb, initially in the $5^2P_{1/2}$ state, will form an $A\,^2\Pi_{1/2}$ molecular state of Rb-Xe*. The resulting intermolecular potential is attractive.[2] Ground state Rb will form an $X^2\Sigma_{1/2}$ molecular state of Rb-Xe, with a potential that is largely repulsive. The difference potential between these two molecular states is monotonic. Since the difference potential has no extrema, there are only single solutions to Eq. (17). Therefore, electronic transitions between the $A^2\Pi_{1/2}$ and $X^2\Sigma_{1/2}$ molecular states satisfy the criterion of processes considered in this paper. If gaseous Rb is excited to the $5^2P_{1/2}$ atomic state and allowed to collide, photoemission between these molecular states will occur. Since the difference potential is a monotonically increasing function of internuclear distance, this quasimolecular emission will be in the red wing of the 7948-Å atomic line. An experimental spectrum has been obtained showing resolved undulations in the far wing of this line.[2] The availability of this information contributed to the selection of this system for study.

Since the initial $A^2\Pi_{1/2}$ potential is attractive, we must consider what bound diatomic population contributions to the wing emission. Since the excited state is populated at the atomic asymptote, only the free-free transitions will contribute if only binary collisions occur. However, excited diatomic Rb-Xe can form through three body collisions, and subsequently contribute to the red-wing emission. To compare theory with experiment, we would normally have to know what is the contribution of the bound population at thermal energies. But in the limit of zero pressure, the emission is totally due to free-free binary collisions, since teratomic collisions are so rare. Fortunately, an experimental spectrum was obtained for this limit at a temperature of 300 °K.[2] Thus, we can safely use a thermal average over initial states that are asymptotically free. We should point out that the uniform JWKB uniform approximation can also be applied to bound states with some appropriate modifications.

Although theoretical Rb-Xe potentials are available,[19] they were not employed in the present calculations. It is known that they do not always produce a difference potential consistent with experimental results when A or B molecular states are involved.[20,21] There is very good agreement, however, between theoretical and semiempirical potentials for the X state. Therefore, semiempirical potentials were selected for both the A and X states. In atomic units, the analytic equation used for the $A^2\Pi_{1/2}$ potential for all range of R is[22]

$$V_i(R) = 2.87\times10^{-3}(\{\exp[-0.652(R-6.52)]-1\}^2 - 1 - 0.168\{1-\exp[(R/13.23)^{12}]\}\times(13.23/R)^6)\,. \quad (26)$$

The radius R is in units of bohr (1 bohr = 0.529 $\times 10^{-8}$ cm), and the potential energy is in units of hartree (1 hartree = 4.360×10^{-11} erg = 27.211 eV = 2.195×10^5 cm^{-1}). A least-squares analytic fit was sought for the semiempirical $X^2\Sigma_{1/2}$ poten-

tial.[2] The final form employed in the computations was (again in atomic units):

$$V_f(R) = -5.821\times10^{-4} + 2.5903\times10^{-4}(R-8.88)^2 + 6.20408\times10^{-5}(R-8.88)^3 + 3.50597\times10^{2}\exp(-1.905\times R)\ . \quad (27)$$

This was used for radii up to 9.45 bohr. Beyond that, an inverse 6 – 8 potential was smoothly mated to it, $V_f(R) = -2.07700\times10^{2}\,R^{-6} - 1.20577\times10^{4}R^{-8}$. The asymptotic difference between the A and X potentials is 0.0572760 hartree; i.e., $\Delta V_{if}(\infty) = 0.0572760$. This is the energy of the 7948 Å atomic line of Rb. We will assume the transition dipole moment [$M(R)$ in Eq. (1)] is constant.

To produce a theoretical spectrum that can be compared to experimental results, we must calculate a Maxwellian average over initial energies of the free nuclei. The averaged spectrum (intensity per unit frequency interval) is given by

$$I_\nu(\lambda) = \frac{2\pi}{(\pi kT)^{3/2}}\int_0^\infty \frac{dI}{d\nu}(E,\lambda)E^{1/2}\exp\left(\frac{-E}{kT}\right)dE\ . \quad (28)$$

In Eq. (28), k is Boltzmann's constant. This is in a form to which we can apply the Gauss-Laquerre quadrature method. The appropriate quadrature formula is

$$\int_0^\infty f(x)\exp(-x)dx = \sum_{n=1}^{N} A_n f(x_n)\ ,$$

which is exact if $f(x)$ is a polynomial of degree $2N-1$ or less. The A_n and x_n are tabulated numbers that depend on N.[23] We see that $E_n = kT\,x_n$. Choosing $N=4$, we find $E_1 = 3.075\times10^{-4}$ hartrees, $E_2 = 1.6643\times10^{-3}$ hartrees, and $E_3 = 4.3249\times10^{-3}$ hartrees for a temperature of $T = 300$ °K. It was unnecessary to calculate the contribution from $E_4 = 8.9567\times10^{-3}$ hartree because of the smallness of $A_4 f(x_4)$.

The differential intensities for these three initial kinetic energies are displayed in Fig. 1. The wavelength interval, 8100–8600 Å, covers most of the far red wing of the 7984-Å line that is of interest. Note that the intensity scale is logarithmic base 2. The intensity spectrum produced at an incident energy E_n has been multiplied by a factor of 2^n to spread out the three spectra so as not to clutter the graph. The normalization constant I_n will be discussed later.

The undulatory structure so readily apparent at the lowest energy (E_1) is considerably less evident at the higher energies. If we smooth out the undulations in all the spectra, though, we notice that changes in kinetic energy do not greatly affect the spectrum (at least in this thermal range). The

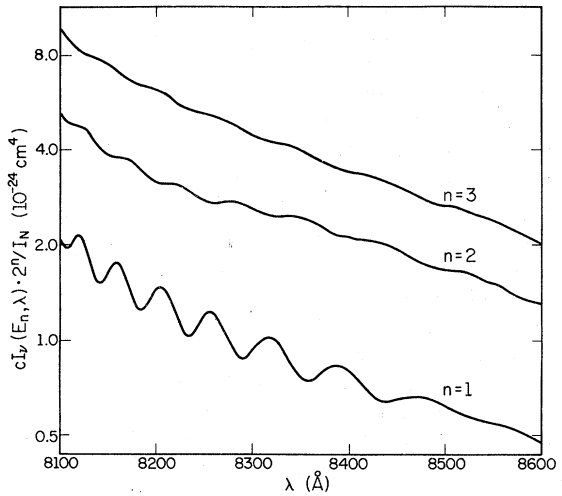

FIG. 1. Calculated differential emission spectra for the free-free $A^2\Pi_{1/2}\rightarrow X^2\Sigma_{1/2}$ transition in RbXe at three different collisional energies. n is the collisional energy index: $E_1 = 3.075\times10^{-4}$ hartrees (0.008367 eV), $E_2 = 1.6643\times10^{-3}$ hartrees (0.045287 eV), and $E_3 = 4.3249\times10^{-3}$ hartrees (0.11768 eV). The factor 2^n is introduced to make comparisons between spectra easier. The quantity displayed cI_ν/I_N was chosen to facilitate comparison with the experimental quantity reported in Ref. 2.

magnitude of the differential intensity remains about the same at each wavelength, and retains its characteristic as a decreasing function of wavelength.

To explain the changes in the undulatory pattern, we must consider the effect that changes in angular momentum has on the T-matrix elements. As L increases, the local wave number [Eq. (5c)] at each internuclear separation decreases. At the same time, the classical turning points move outward. These two things imply that the phase [Eq. (5d)] and its derivative are decreasing functions of angular momentum. Consequently, the same generally applies to the phase difference that controls the oscillations in the T-matrix elements [Eq. (20)]. These effects are progressively more significant as L increases because the centrifugal term in the local wave number becomes more comparable to the constant local kinetic energy, $E - V_c(R)$. From this we can predict some general relationships between oscillations in the T-matrix elements and changes in the collisional angular momentum of the nuclei.

We expect the extrema of the oscillations to move away from the classical turning points as L increases. At each stationary phase point, the phase difference is decreasing and this effect is cumulative as we move away from the turning points. The changes should be largest nearer the turning point

because the smaller phases are more affected by the centrifugal terms. Finally, we expect these effects should be more pronounced at higher values of L than at lower.

To correlate this analysis with the actual spectrum, we note that the difference potential is a monotonically increasing function of internuclear distance. From Eq. (17) this means that shorter wavelengths correspond to stationary-phase points at greater radial distances. Consequently, classically allowed transitions with shorter wavelengths are farther from classical turning points than those with longer wavelengths. From our previous discussion, we conclude that the peaks of the T-matrix elements should shift toward shorter wavelengths as L increases, that the frequency of oscillations as a function of wavelength should decrease, and that these effects are larger at longer wavelengths.

To confirm this, we examine the change in the spectra at a single energy as we include more and more angular momenta in Eq. (1); i.e., as we increase L_{max}, the maximum angle momentum. A number of these partial-sum spectra at the energy E_2 are shown in Fig. 2. Note that the intensity

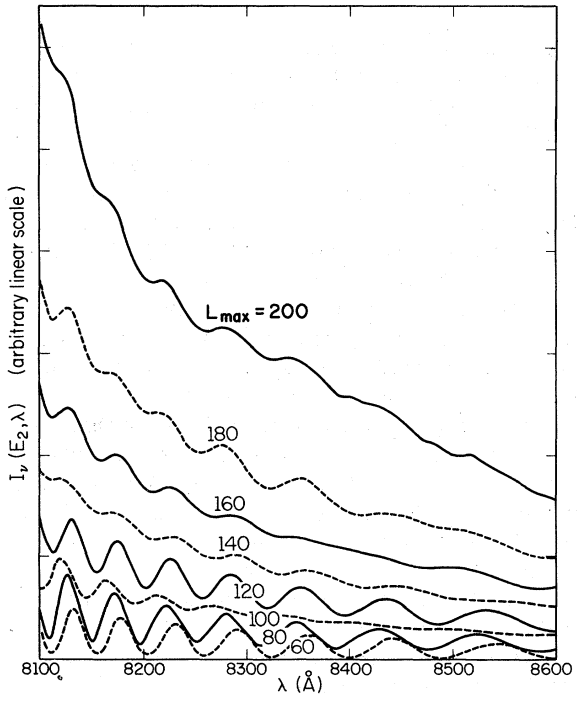

FIG. 2. Partial-sum emission intensities at a single collisional energy, $E_2 = 1.6643 \times 10^{-3}$ hartrees (0.045287 eV). L_{max} is the largest value of the orbital angular momentum included in the partial sum of the differential intensity [Eq. (1)]. Note that unlike Fig. 1, the intensity scale is linear, not logarithmic.

scale is linear on this graph. We observe the expected behavior between $L_{max} = 60$ and 100; the maxima shift to shorter wavelengths, with the greatest shift occurring at longer wavelengths. However, from $L_{max} = 120$ to 200, the extrema remain at about the same positions they occupied at $L_{max} \approx 80$. Beginning around $L_{max} \approx 100$, the depth of the undulations is strongly affected by changing L_{max}, sometimes being shallow, sometimes deep.

Up to $L \approx 80$, the undulations shift very little because $E - V_c(R) \gg [\hbar^2(L+\frac{1}{2})^2/R^2]/2\mu$. However, between $L = 80$ and $L = 100$, the centrifugal term is large enough to shift the maxima of the T-matrix elements to wavelengths at which there were zeroes at lower values of L. The T-matrix elements at larger L make a greater contribution to the partial sum of Eq. (1) due to the weighting factor of $2L+1$. Thus, the shifted T-matrix elements fill in the minima of the prior undulatory structure to produce the much-smoothed spectra seen at $L_{max} = 100$. As L_{max} now increases, the positions of oscillations in the T-matrix elements are rapidly shifting to shorter wavelengths as the classical turning points move to greater internuclear distances. This means that, for some L_{max}, most of the maxima of the newly-added matrix elements ($L \gtrsim 80$) coincide with the maxima of the partial-sum spectra at $L_{max} = 80$; for other values of L_{max} most of the maxima coincide with the minima of the $L_{max} = 80$ spectra. Thus the strength of the undulations is sometimes enhanced, sometimes tempered. Since the added "shifting" undulations are never large or stable enough to swamp the structure produced up to $L = 80$, the undulations established at $L_{max} \approx 80$ persists in the spectra for all larger L_{max}. Between $L = 200$ and 210, the stationary phase points enter one-by-one the classical forbidden regions of the effective potentials as the turning points move rapidly outward. By $L = 210$, the contributions from the T-matrix elements are at least ten orders of magnitude less than the partial sum. Thus the final spectra is, effectively, that produced by the partial sum of $L_{max} = 210$. On the scale used in Fig. 2, there is no detectable difference between the partial-sum spectrum at $L_{max} = 200$ and $L_{max} = 210$. The end result of the "shifting" T-matrix elements is the smoothing out of the undulations established at lower angular momenta. At the higher energy of E_3, even more angular momenta contribute to the final spectrum and more filling in occurs. That is why the undulations at E_3 are even less pronounced than those at E_2.

This analysis leads directly the explanation of the prominent undulatory pattern seen at the lowest energy E_1 in Fig. 1. At that energy, a

centrifugal barrier develops that is higher than the incident kinetic energy. The colliding particles begin penetrating this barrier at $L=127$, at a radial separation greater than any of the stationary points for the wavelength interval 8100–8600 Å. Nuclei are then prevented from getting into the inner well region with any significant probability. Thus, the partial sum is effectively terminated rather suddenly. If we now return to Fig. 2, we see that between $L_{max}=80$ and 120, the partial-sum spectrum changes from having a pronounced undulatory structure to a shallow one, and back again for energy E_2. We expect a similar behavior may occur at the lower energy E_1. In fact this does happen between $L_{max}=100$ and $L_{max}=126$. At $L_{max}=100$ and $L_{max}=126$, the partial-sum spectra has a much more pronounced undulatory spectra then at $L_{max}=120$. Consequently, if barrier penetration had commenced at $L=120$ instead of $L=126$, the spectra at energy E_1 would have a weak undulatory pattern rather than a strong one. Therefore, for incident energies near E_1, the spectrum will sometimes have prominent undulations, sometimes not.

At higher energies, such as E_2 and E_3, the incident kinetic energy is always larger than the centrifugal barrier at all L. By the time the stationary-phase points enter the classically forbidden region, the inner well in the effective potential has disappeared. Thus a complete range of local wave numbers are represented in the sum of Eq. (1), from the maximum (at $L=0$) to a minimum of zero. The structure of the partial-sum spectra will not change much for small changes in initial kinetic energy, since the complete range of wave numbers is always covered. However, at lower energies, like E_1, the partial sum is abruptly terminated by onset of barrier penetration before all the wave numbers are covered. Changing the incident energy by the same small amount can have a significant effect on which wave numbers are represented. This modulates the strength of the undulatory structure at these energies. At even lower energies, the undulatory structure, will again be less sensitive to changes in incident energy. Because the initial potential is attractive, there will be a range of low incident energies for which the partial-sum spectra is stable to increasing L_{max} to its termination by centrifugal barrier penetration.

From all this, we conclude that persistent undulations in the spectra are produced from values of angular momenta that are small enough not to effect appreciably the prior partial-sum spectra. The general condition is $E - V_c(R_s) \gg \hbar^2(L+\frac{1}{2})^2/(2\mu R_s^2)$. Once this condition is no longer met, further summation of the partial sum may change the strength of the undulations, but will not affect the positions very much. Generally, the larger the fraction of angular momenta that satisfies this condition, the more prominent the undulations in the complete spectrum.

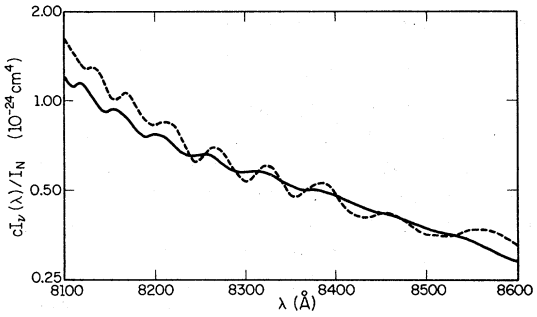

FIG. 3. Comparison of the calculated (solid line) and experimental (dashed line) red-wing emission spectra of RbXe* at a temperature of 300 °K in the zero-pressure limit. I_N represents the total integrated intensity for the entire line profile. The quantity $cI_\nu(\lambda)$ used here is the same as the experimental quantity $I(k)/[\mathrm{Xe}][\mathrm{Rb}^*]$ reported in Ref. 2.

V. RbXe* ($A^2\pi_{1/2}$) POTENTIAL

With the insights gained above, we can suggest modifications of the RbXe*($A^2\Pi_{1/2}$) potential used thus far by comparing the thermally-averaged theoretical spectrum with the experimental one. These are shown together in Fig. 3. Note the normalized intensity scale is again $\log_2$. The theoretical normalization constant I_N used in Figs. 1 and 3, was adjusted to bring the thermally-averaged theoretical magnitudes into good "eyeball" agreement with the normalized experimental spectrum.[2] It represents the integrated intensity over the entire broadened-line profile, and is effectively the intensity of the atomic line at 7948 Å. We observe that the theoretical spectrum has about the right slope-versus-wavelength relationship, with some deviations for wavelengths shorter then about 8250 Å. We also see that the periods of the undulations are in agreement for wavelengths shorter than 8400 Å, although the theoretical undulations are shifted by about 10 Å to the blue.

The main difference between the two spectra is the much stronger undulations in the experimental one. From the analysis developed in Sec. IV, this implies that we must produce a larger fraction of the final-sum theoretical spectrum that is stable to changes in angular momentum. This can be accomplished in two ways. We can increase the depth of the RbXe* potential well to make the local wave numbers relatively insensitive to changes in angular momentum over a larger range of L, or

we can adjust the potential at larger values of R to terminate the partial sum at a lower value of L_{max}. The wavelength interval discussed here, 8100–8600 Å, corresponds to internuclear separations of 6.53 bohr to 8.29 bohr. This covers the outer half of the RbXe* well region. If we increase the depth of the well, the spacing between undulations will change; it would then be difficult to match up the theoretical undulations with the experimental as well as they now are.

Adjustments to terminate the partial-sum spectra at lower values of L_{max} seem more promising. By increasing the asymptotic potential (decreasing its attraction) for $R \gtrsim 10.0$ bohr, we can raise the centrifugal barrier up to typical thermal energies at lower angular momenta. For instance, if we change the RbXe* potential at 10.0 bohr from its present value of -5.89×10^{-4} hartree to approximately -2.0×10^{-4} hartree, the partial-sum spectra at energy E_2 will be terminated by a centrifugal barrier at $L_{max}\approx180$ instead of $L_{max}=210$. From Fig. 2, we can see that the final spectrum would have much more pronounced undulations.

Although such an adjustment will not change the well region very much, it will tend to decrease its depth somewhat at larger values of internuclear separation. This is the region of shorter wavelengths. We would not expect the period of undulations to change very much since the local wave numbers would not be affected greatly at these stationary-phase points. But we would expect the spectrum to increase in magnitude at the shorter wavelengths relative to that at longer. This is due to the factor of $[2\Delta k'_{fi}(R_s)]^{-1/2}$ found in Eq. (20). Since the final state RbXe($X^2\Sigma_{1/2}$) is repulsive and the initial RbXe*($A^2\Pi_{1/2}$) is attractive in this region, making the RbXe* potential less attractive will decrease $\Delta V'_{fi}(R)$. Since $\Delta k'_{fi}(R_s)$ is directly proportional to $\Delta V'_{fi}(R_s)$, we expect the corresponding increase in magnitude should be more noticeable than any changes in undulatory frequency. Consequently, we would expect that the magnitude of the differential intensity should increase as a function of decreasing wavelength if we smoothly decrease the attraction of the RbXe* potential at larger internuclear distances. This is exactly the change we want to obtain in the theoretical spectrum for wavelengths less than 8250 Å ($R_s>7.57$ bohr).

Finally, we note that the experimental spectrum still exhibits undulations at long wavelengths ($\lambda \gtrsim 8360$ Å), while the theoretical spectrum is smooth. By terminating the partial sum at $L_{max}=180$, we expect some undulatory structure may be preserved at these longer wavelengths (see Fig. 2). However, this would not be sufficient to recreate the strong undulations experimentally observed. To achieve this, we can make the inner-half of the RbXe* well somewhat less repulsive so that the local wave numbers increase somewhat. This will produce a more stable undulatory pattern at these wavelengths. Making the inner core of the potential less repulsive will also increase $\phi_i^L(R_s)$. This will tend to shift the undulatory extrema a little to the red. This may be sufficient to correct the 10-Å discrepancy between the theoretical and experimental spectra previously mentioned. Quantal computations are planned to verify that the uniform-JWKB approximation is accurate enough to warrant its use for such a detailed analysis.

VI. CONCLUDING REMARKS

We have presented a semiclassical approach to calculating the energy spectrum of particles (photons or electrons) emitted in electronic transitions that occur during a particular class of atomic collisions. The method can be used for systems that have monotonic difference potentials. The uniform nature of its derivation assures its applicability even to transitions that occur near classical turning points. Since only phase integrals need to be computed, much computer time is saved relative to quantal procedures. But perhaps more importantly, the uniform-JWKB stationary-phase approximation lends itself to an informative, interpretive analysis of the energy spectrum. As has been illustrated for the RbXe*($A^2\Pi_{1/2}$) potential, the method cannot only be used to test the accuracy of proposed intermolecular potentials, but also can lead to suggestions for consistent improvements in the potentials. These suggestions were derived from a semi-quantitative analysis of the predicted spectrum and the analytic form of T-matrix elements. Obviously, it would be advantageous to invert the mathematical expression for the matrix elements to produce potentials directly from experimental spectra. The development of an analytic means of evaluating spectra is the first necessary step in this direction. In a forthcoming paper, we will examine the detailed accuracy of this semiclassical method by numerically comparing its results with quantal computations.

ACKNOWLEDGMENTS

This work was supported by funds from a National Science Foundation Energy-Related Postdoctoral Fellowship (No. 75-19947). The author would like to thank the University of California, Berkeley, for supplying most of the computer time used in this research project. William

H. Miller graciously sponsored the author's visit at that institution. The author would also like to express his appreciation to Alan Gallagher, Joint Institute for Laboratory Astrophysics, for a number of informative discussions about the physical processes considered in this paper.

APPENDIX

To calculate the overlap integral of two general, regular homogeneous Airy functions, we being with the integral:

$$I=\int_{-\infty}^{\infty} 2\pi(3p)^{-1/3}\mathrm{Ai}[(3p)^{-1/3}(R+\alpha)]\,2\pi(3q)^{-1/3} \times \mathrm{Ai}[(3q)^{-1/3}(R+\beta)]\,dR\ . \tag{A1}$$

Using the integral form of the Airy function[15]

$$\mathrm{Ai}[(3a)^{-1/3}u] = (2\pi)^{-1}(3a)^{1/3} \times \int_{-\infty}^{\infty} \exp[i(at^3+ut)]\,dt\ , \tag{A2}$$

we find that

$$I=\iiint_{-\infty}^{\infty} \exp[i(px^3+Rx+\alpha x+qy^3+Ry+\beta y)]\,dx\,dy\,dR\ . \tag{A3}$$

By noting that the integral form of the Dirac delta function is

$$\int_{-\infty}^{\infty} \exp[i(x+y)R]\,dR = 2\pi\delta(x+y)\ ,$$

we see that

$$I = 2\pi\int_{-\infty}^{\infty} \exp\{i[(p-q)x^3+(\alpha-\beta)x]\}\,dx \tag{A4a}$$

$$= (2\pi)^2(3p-3q)^{-1/3}\mathrm{Ai}[(3p-3q)^{-1/3}(\alpha-\beta)]\ . \tag{A4b}$$

By setting $(3p)^{-1/3}=a$ and $(3q)^{-1/3}=b$, and then rearranging the equality between Eq. (A1) and Eq. (A4b) we arrive at the desired goal

$$\int_{-\infty}^{\infty} \mathrm{Ai}[a(R+\alpha)]\,\mathrm{Ai}[b(R+\beta)]\,dR = (ab)^{-1}\left(\frac{1}{a^3}-\frac{1}{b^3}\right)^{-1/3}\mathrm{Ai}\left[\left(\frac{1}{a^3}-\frac{1}{b^3}\right)^{-1/3}(\alpha-\beta)\right]. \tag{A5}$$

[1] C. L. Chen and A. V. Phelps, Phys. Rev. A 7, 470 (1973).
[2] C. G. Carrington and A. Gallagher, J. Chem. Phys. 60, 3436 (1974).
[3] C. G. Carrington and A. Gallagher, Phys. Rev. A 10, 1464 (1974).
[4] J. Cooper, JILA Report No. 111 (University of Colorado 1973) (unpublished).
[5] K. M. Sando and J. C. Wormhoudt, Phys. Rev. A 7, 1889 (1973).
[6] J. Szudy and W. E. Baylis, J. Quant. Spectrosc. Radiat. Transfer 15, 641 (1975).
[7] R. J. Bieniek, Chem. Phys. Lett. 40, 72 (1976). The difference potential defined just prior to Eq. (7) in this reference should read $\Delta V(R_n)=V_i(R_n)-V_f(R_n)$. More importantly, the variable u_n, defined just after Eq. (9), should read $u_n=a_n+2c_n^3/(27d_n^2)$.
[8] M. V. Berry and K. E. Mount, Rep. Prog. Phys. 35, 315 (1972).
[9] M. S. Child, Mol. Phys. 29, 1421 (1975).
[10] J. B. Gerado and A. W. Johnson, J. Appl. Phys. 44, 4120 (1973).
[11] J. J. Ewing, Proc. Soc. Photo-Opt. Instrum. Eng. (Ultra High Power Lasers for Practical Appl.) 76, 133 (1976).
[12] W. F. Krupke and E. V. George, Proc. Soc. Photo-Opt. Instrum. Eng. (Ultra High Power Lasers for Practical Appl.) 76, 22 (1976).
[13] L. I. Schiff, *Quantum Mechanics* (McGraw-Hill, 1968).
[14] R. G. Gordon, J. Chem. Phys. 51, 14 (1969).
[15] M. Abramowitz and I. A. Stegun, *Handbook of Mathematical Functions* (Dover, New York, 1965).
[16] W. H. Miller, J. Chem. Phys. 48, 464 (1968).
[17] R. G. Gordon, J. Chem. Phys. 52, 6211 (1970).
[18] R. J. Bieniek, Ph.D. dissertation (Harvard University, 1975) (unpublished).
[19] J. Pascale and J. Vanderplanque, J. Chem. Phys. 60, 2278 (1974); and *Molecular Terms of the Alkali-Rare Gas Atom Pairs: Numerical Results and Potential Energy Curves, IV-Rubidium* (Service de Physique Atomique, Centre d'Etudes Nucleaires de Saclay, France, 1974).
[20] R. Scheps, C. Ottinger, G. York, and A. Gallagher, J. Chem. Phys. 63, 2581 (1975).
[21] R. J. Bieniek and A. Dalgarno, Bull. Am. Phys. Soc. 19, 1174 (1974).
[22] G. York, R. Scheps, and A. Gallagher, J. Chem. Phys. 63, 1052 (1975). Although this paper mainly deals with Na-rare gas potentials, it gives revised parameters for the Rb-Xe* potential in Table I.
[23] F. Scheid, *Numerical Analysis* (McGraw-Hill, New York, 1968).